

# Redshifts and Velocity Dispersions of Galaxy Clusters in the Horologium-Reticulum Supercluster

Matthew C. Fleenor, James A. Rose, Wayne A. Christiansen

*Department of Physics & Astronomy, University of North Carolina, Chapel Hill, NC 27599*

fleenor2@physics.unc.edu, jim@physics.unc.edu, wayne@physics.unc.edu

Melanie Johnston-Hollitt

*Department of Physics, University of Tasmania, TAS 7005, Australia*

Melanie.JohnstonHollitt@utas.edu.au

Richard W. Hunstead

*School of Physics, University of Sydney, NSW 2006, Australia*

rwh@physics.usyd.edu.au

Michael J. Drinkwater

*Department of Physics, University of Queensland, QLD 4072, Australia*

mjd@physics.uq.edu.au

and

William Saunders

*Anglo-Australian Observatory, Epping NSW 1710, Australia*

will@aaoepp.aao.gov.au

## ABSTRACT

We present 118 new optical redshifts for galaxies in 12 clusters in the Horologium-Reticulum supercluster (HRS) of galaxies. For 76 galaxies, the data were obtained with the Dual Beam Spectrograph on the 2.3m telescope of the Australian National University at Siding Spring Observatory. After combining 42 previously unpublished redshifts with our new sample, we determine mean redshifts and velocity dispersions for 13 clusters, in which previous observational data were sparse. In six of the 13 clusters, the newly determined mean redshifts differ by more than  $750 \text{ km s}^{-1}$  from the published values. In the case of three clusters, A3047, A3109, and A3120, the redshift data indicate the presence of multiple components along the line of sight. The new cluster redshifts, when combined with other reliable mean redshifts for clusters in the HRS, are found to be distinctly bi-modal. Furthermore, the two redshift components are consistent with the bi-modal redshift distribution found for the inter-cluster galaxies in the HRS by Fleenor et al. (2005).

*Subject headings:* galaxies: clusters: general, large-scale structure

## 1. INTRODUCTION

The Horologium-Reticulum supercluster (HRS) is an extended region of high galaxy density (Shapley 1935; Lucey et al. 1983; Einasto et al. 2003; Fleenor et al. 2005), covering  $\sim 150$  square degrees of sky at a mean redshift of  $\sim 20,000 \text{ km s}^{-1}$ . The HRS also contains more than 20 galaxy clusters (Einasto et al. 1997, 2002). As discussed in Hudson et al. (1999) and Einasto et al. (2001), the HRS is the second largest mass concentration within  $\sim 300 \text{ Mpc}$ , where it is only surpassed by the Shapley supercluster (SSC).

While the SSC has been extensively studied (Quintana et al. 1995, 2000; Drinkwater et al. 1999, 2004; Bardelli et al. 1998, 2000), the HRS remains relatively unexplored. Due to the potential importance of such a large-scale structure in the present-epoch universe, we have embarked on a redshift survey to provide a comprehensive mapping of the HRS. Our initial results, which contain 547 galaxy redshifts in the *inter-cluster* regions of the HRS, are reported in Fleenor et al. (2005, hereafter Paper I). A key result from Paper I is that the distribution of inter-cluster galaxies is separated into two distinct redshift components. On the other hand, the published mean redshifts for 21 galaxy clusters in the HRS do not exhibit such a bi-modal distribution. The differing results between the cluster and inter-cluster redshift distributions appear to contradict the view that galaxy clusters share the kinematics of the inter-cluster galaxy distribution as a result of their location at intersecting filaments of galaxies (e.g., van Haarlem & van de Weygaert 1993; Bond et al. 1996; Colberg et al. 1999, 2005). However, the mean redshift for many of these clusters is based on fewer than four galaxy redshifts per cluster, i.e., sparse information. To clarify the distribution of cluster redshifts in the HRS, we have obtained new data for 12 clusters in which the previously published data were sparse. The results of this program are reported below and, when combined with other previous redshift data, give an improved assessment of the distribution of cluster redshifts in the HRS. Throughout the paper, we adopt the following cosmological parameters:  $\Omega_m = 0.3$ ,  $\Omega_\Lambda = 0.7$ , and  $H_o = 70 \text{ km s}^{-1} \text{ Mpc}^{-1}$ , which implies a spatial scale of  $4.6 \text{ Mpc degree}^{-1}$  ( $77 \text{ kpc arcmin}^{-1}$ ) at the  $\sim 20,000 \text{ km s}^{-1}$  mean redshift of the HRS.

## 2. CLUSTER SAMPLE

Lists of galaxy clusters in the region of the HRS have been taken from two major studies. The first is the Abell catalog (extension) (hereafter ACO in Abell et al. 1989), while the second is the Automated Plate Measuring Machine cluster catalog (hereafter APMCC in Dalton et al. 1994, 1997). Since galaxy clusters represent the largest (at least partly) virialized structures, they serve as massive signposts for identifying and studying superclusters of galaxies. Based on the ACO, Zucca et al. (1993) identified 18 HRS clusters using a combination of partial redshift information and percolation algorithms. While working with the same list of ACO clusters, Einasto et al. (1994) identified 26 members of the HRS. In Paper I, we used the 17 ACO clusters occurring in both studies to define the mean redshift of the HRS ( $\bar{z} = 19,900 \text{ km s}^{-1}$ ), and we adopted the FWHM of the cluster redshift distribution as defining the HRS kinematic core to lie between  $17,000$  and  $22,500 \text{ km s}^{-1}$  (see Figure 4, Paper I). However, the mean redshifts are uncertain for 10 of the 17 ACO clusters because they are based on fewer than four galaxy redshifts each ( $N_{\text{gx}} < 4$  in Struble & Rood 1999, hereafter SR99). In this paper we report new spectroscopic observations, together with previously unpublished redshifts, for 9 of these 10 clusters with the aim of determining a more accurate mean redshift and dispersion for each cluster. Published data for the tenth cluster, A3109, have been reassessed, and additional spectra have been obtained for a further three clusters with sparse data in the literature.

Figure 1 shows the spatial locations of the thirteen clusters in this study as dotted circles. A further 15 clusters with secure redshifts, based on 10 or more galaxies, are also displayed; those that fall within the kinematic core of the HRS are shown as solid-line open circles. Clusters that fall outside the statistically-defined kinematic core may still, in fact, be members of the larger supercluster complex. Of the thirteen clusters in the current study, eleven are ACO, Richness 0 clusters, and the remaining two are from the APMCC. Since the values of cluster richness for the APMCC are not assigned in the same way as the ACO, comparative determinations were taken from Einasto et al. (2001) for the two APMCC clusters, and

they were found to be similar to ACO Richness 0.

### 3. OBSERVATIONS AND REDUCTIONS

Spectroscopic observations were conducted 2004 November 14–17 with the 2.3m telescope of the Australian National University (ANU) at Siding Spring Observatory. The Dual Beam Spectrograph (DBS) was utilized in conjunction with a coated SiTE 1752×532 CCD. The 300B grating was used with all light directed into the blue arm via the insertion of a reflective mirror instead of the customary dichroic. With a central wavelength of 5200 Å, the above arrangement yielded a dispersion of 2.18 Å pix<sup>-1</sup> from [OII]λ3727 through Mg Ibλ5175 for the mean redshift of the HRS. Wavelength calibration was based on CuAr lamp exposures carried out after each object exposure. For each observation, the spectrograph was rotated to place two or more galaxies on the slit. Galaxies were selected based on their spatial proximity and their apparent brightness. Specifically, all galaxies within a spatial radius of ≤ 15′ (= 0.5R<sub>Abell</sub> ∼ 1 Mpc) to the published cluster center were examined and arranged in order of decreasing brightness. We targeted only those galaxies with a blue, *b<sub>J</sub>*, magnitude brighter than 18.25, as given in the SuperCOSMOS catalog (Hambly et al. 2001). With a typical exposure time of 30 minutes, all spectra had signal-to-noise ratios of 15:1 or greater and yielded accurate redshift determinations.

Object exposures were reduced in the standard manner via the IRAF<sup>1</sup> software package. Specifically, the following steps were completed: debiasing, flat fielding, sky subtraction, cosmic-ray removal, and wavelength calibration. Cosmic rays were removed using the variance weighting option in the `apall` routine for aperture extraction. For those objects with multiple exposures, the reduced spectra were co-added. In all, 76 usable galaxy spectra were obtained over the four nights of observations, and they are listed in Table 1 with their determined redshift and associated uncertainty. Because the spectrograph position angle was adjusted to allow two galaxies to be centered on the slit, observations did not occur at the parallactic angle, and the uncertainty from atmospheric dispersion could in principle be as much as 40 km s<sup>-1</sup>. Radial velocities were determined for

the galaxy spectra by the standard technique of cross-correlating the galaxy spectra against those of template stars. Stellar spectra of the G8III star HD 80499 and of the G4V star HD 106116 from the Indo-US Coudé Feed Spectral library (Valdes et al. 2004) and two de-redshifted DBS stellar spectra (the G0 star HD 33771 and a serendipitous Galactic G dwarf at  $\alpha_{J2000} = 03:29:38.44$  and  $\delta_{J2000} = -52:36:08.5$ ) were utilized as templates for the redshift determination using the `xvsao` routine. Only cross-correlation fits with  $R > 4$  (Tonry & Davis 1979) were considered reliable and then averaged. For the ten galaxies with emission-dominated features, procedures were followed in a manner similar to that detailed previously in Paper I. As a final step, all redshifts were corrected to the heliocentric reference frame.

In addition to the new data from the ANU/DBS, 42 galaxy redshifts for various clusters in our sample were obtained from other sources. Eighteen cluster galaxies were observed during our survey with the multi-fiber, 6° field instrument (6dF, Parker et al. 1998) on the UKST in 2004 November. Although that survey focused on the inter-cluster galaxies in the HRS, otherwise unused fibers were placed on galaxies within the clusters themselves. UKST/6dF spectra covered the wavelength range from 3900–7600 Å and yielded average instrumental resolutions of 4.9 Å and 6.6 Å, for the 580V and 425R gratings respectively. The automatic 6dF data reduction package completed the following: debiasing, fiber extraction, cosmic-ray removal, flat-fielding, sky subtraction, wavelength calibration, splicing, and co-addition (Jones et al. 2004). The optical redshift for each galaxy was determined via the semi-automated `runz` software (Colless et al. 2001), which employed both cross-correlation for absorption features and emission-line matching for typical features (e.g., [OII]λ3727, [OIII]λ4959/5007, and Balmer lines).

Furthermore, two previously unpublished datasets obtained with the Anglo-Australian Telescope (AAT) were relied on for establishing properties of certain clusters. Specifically, T. Mathams used the fibre-optic-coupled aperture plate system (FO-

<sup>1</sup>Image Reduction and Analysis Facility (IRAF) is written and supported by the National Optical Astronomy Observatories (NOAO) and the Association of Universities for Research in Astronomy (AURA), Inc. under cooperative agreement with the National Science Foundation.

CAP, see Gray 1983) during 1986–1988 to observe galaxies within A3123 and APMCC 421 with a dispersion of  $\sim 2 \text{ \AA pix}^{-1}$  from 3600–5600  $\text{\AA}$ . I. Klamer used the  $2^\circ$  field instrument (2dF, Lewis et al. 2002) in 2002 January to observe galaxies within A3104 with  $\sim 4 \text{ \AA pix}^{-1}$  (or 8  $\text{\AA}$  FWHM) from 3600–8000  $\text{\AA}$ . The overlap of 270 galaxies between the Mathams dataset and the observations from Rose et al. (2002) revealed a velocity offset of  $80 \text{ km s}^{-1}$  within the Mathams dataset. Therefore, a correction of  $-80 \text{ km s}^{-1}$  was applied to all redshifts cited by Mathams.

The results of our observations, together with the other previously unpublished data, are summarized in Table 1. The first column contains the galaxy ID, while columns (2) and (3) list the J2000 coordinates, and column (4) gives the SuperCOSMOS  $b_J$  magnitude. In column (5) we give the velocity ( $cz$ ) and its associated uncertainty obtained from our ANU/DBS spectra. The iterative method of calculating the mean cluster redshift and velocity dispersion (described in §4) shows that some galaxies are either foreground or background to the cluster. We label those galaxies with an asterisk (\*) in column (5). Galaxy redshifts from the literature (via the NASA Extragalactic Database, NED) are also utilized in our calculations. All previously existing redshifts, either published or unpublished, are listed in column (6) with their respective source in column (7).

#### 4. DETERMINATION OF MEAN CLUSTER REDSHIFTS AND DISPERSIONS

Given that galaxy clusters are thought to form via accretion along intersecting filaments (e.g., West & Blakeslee 2000), and that such processes are particularly pronounced in a dense environment like the HRS, we expect the assumption of a gaussian velocity distribution for the galaxies within the HRS clusters to be problematic. Specifically, the probability of both projected and truly overlapping groups and/or clusters will be enhanced within the supercluster environment. Furthermore, the calculation of the cluster mean redshift and velocity dispersion under an assumption of gaussian statistics is neither robust nor efficient (Pearson 1931; Box 1953). Beers et al. (1990, hereafter BFG90) define a number of reliable estima-

tors for the mean cluster redshift (location) and dispersion (scale) that are more robust to the presence of outliers and less wed to the gaussian assumption. For a small number of galaxy redshifts per cluster ( $N_{\text{gx}} < 20$ ), we utilize the biweight estimator for calculating both the location ( $C_{\text{BI}}$ ) and the scale ( $S_{\text{BI}}$ ) of each cluster according to the following:

$$C_{\text{BI}} = M + \frac{\sum_{|u_i| < 1} (x_i - M)(1 - u_i^2)^2}{\sum_{|u_i| < 1} (1 - u_i^2)^2}, \quad (1)$$

where  $M$  is the sample median and  $u_i$  are the individual weights as defined by:

$$u_i = \frac{(x_i - M)}{c(\text{MAD})}. \quad (2)$$

The tuning constant,  $c$ , establishes the low and high velocity cutoff for each cluster. The median absolute deviation, MAD, is defined by:  $\text{MAD} = \text{median}(|x_i - M|)$ . Improvements are made in the final location (and scale) of the cluster by iteratively substituting the most recently calculated  $C_{\text{BI}}$  for the value of  $M$ , and then re-calculating a new  $C_{\text{BI}}$  until convergence is achieved (BFG90). Although we experimented with different values of  $c$  to evaluate the sensitivity of the results on that parameter, the  $c$  parameter was held at the suggested value of 6.0, which excludes all data that are more than 4 standard deviations from the central location. While  $c$  was varied from 4.0 – 10.0 for the  $C_{\text{BI}}$  parameter, the maximum change observed for each cluster remained within the estimated uncertainty of  $C_{\text{BI}}$  in Table 2 (column 8).

In a similar way, the biweight estimator for scale,  $S_{\text{BI}}$ , is given by:

$$S_{\text{BI}} = n^{1/2} \frac{[\sum_{|u_i| < 1} (x_i - M)^2 (1 - u_i^2)^4]^{1/2}}{|\sum_{|u_i| < 1} (1 - u_i^2)(1 - 5u_i^2)|}, \quad (3)$$

with the same definitions as above only here, as suggested,  $c$  was set to 9.0. Again, the routine was iterated until convergence. Moreover, varying  $c$  from 5.0 – 11.0 resulted in a typical total scale change of only  $\Delta S_{\text{BI}} \leq 50 \text{ km s}^{-1}$ . Although BFG90 adopt the terminology of “location” and “scale” because of the difference in definition between these parameters and the canonical mean and dispersion, we retain the common usage of the cluster mean redshift and velocity dispersion for the rest of the paper.

Data on the cluster mean redshifts (location) and velocity dispersions (scale) are summarized in Table 2. The previously published value for the mean redshift is given in column (5), with the source for that redshift in column (6). In column (7) we list the number of galaxies (i.e., those from Table 1, columns (5) and (6), excluding foreground and background galaxies) on which our new mean redshift is based. The new cluster redshift and associated uncertainty are given in column (8). Finally, the newly determined velocity dispersion is given in column (9). For the three cases in which the cluster appears to consist of multiple components, and thus has a less-reliable mean redshift and  $\sigma$ , we have followed the values in column (8) and (9) with a colon (:). These three special cases are discussed further in § 5.

For the remaining ten clusters in the study, the new observations provide a sufficient increase in the number of known redshifts to allow us to determine a reasonably secure velocity dispersion. Furthermore, all of the clusters are Abell richness class,  $R = 0$  (or APMCC equivalent), hence we can assess the mean and scatter in velocity dispersion for  $R = 0$  clusters in the HRS. Given the modest size of our sample of cluster velocity dispersions, we utilize the same routine for the bi-weight location estimator,  $C_{BI}$ , to determine an effective mean velocity dispersion for our cluster sample. After excluding three values as outliers, the remaining ten clusters give a mean velocity dispersion of  $420 \pm 50 \text{ km s}^{-1}$  for Richness 0 clusters. This result is intermediate between published values for galaxy groups (both loose at  $165 \text{ km s}^{-1}$  in Tucker et al. (2000) and compact at  $\sim 250 \text{ km s}^{-1}$  in Hickson (1997)) and rich galaxy clusters (i.e., larger structures) at  $\sim 700 \text{ km s}^{-1}$  (Mazure et al. 1996).

## 5. RESULTS FOR INDIVIDUAL CLUSTERS

The new observational data in three clusters result in velocity dispersions that are quite large in comparison with the  $\sim 400 \text{ km s}^{-1}$  mean value for Richness 0 clusters found above. Although Mazure et al. (1996) find a large intrinsic scatter in velocity dispersion for rich clusters, the derived dispersions for these three clusters rival (and exceed) the *upper* limits observed by the same authors for  $R$

$\geq 1$  clusters. Therefore, the presence of multiple components and/or spatial projection of multiple clusters/groups is suggested. We examine these three systems in greater detail, since their true composition remains unclear.

### 5.1. Abell 3047/ APMCC 290 ( $02^h 45^m 25 - 46^\circ 26'0$ )

The structure of this  $R = 0$ ,  $D = 6$  cluster is quite regular in shape and centers around the brightest cluster galaxy (BCG), 2MASX J02451334–4627194 ( $b_J = 16.68$ ), whose previously published redshift is  $27,581 \text{ km s}^{-1}$  (Grazian et al. 2002). We observe a redshift of  $28,279 \pm 65 \text{ km s}^{-1}$  for the same galaxy, where the difference is most likely due to the higher resolution of the DBS spectra ( $4.5 \text{ \AA}$  compared to  $15\text{--}20 \text{ \AA}$ ). This result is consistent with the mean cluster redshift given in SR99 of  $0.0950$  ( $28,500 \text{ km s}^{-1}$ ), which is based on fewer than 4 galaxy redshifts (“ $N_{gx} < 4$ ”). X-ray emission is also detected at a level of  $L_x = 3.86 \times 10^{43} \text{ ergs s}^{-1}$  (Crudace et al. 2002) and is centered on the BCG, thereby strengthening the idea that at least one significant cluster is present.

The iterative biweight estimator routine does not exclude any of the 8 proposed members, and the following results are obtained:  $\overline{cz} = 27,382 \text{ km s}^{-1}$  and  $\sigma = 1225 \text{ km s}^{-1}$ . While the mean redshift of the cluster is somewhat similar to the previous result for the BCG, the derived velocity dispersion is too inflated for a cluster of Richness 0. In seeking an alternative explanation, we notice that three of the four brightest galaxies have a noticeably different recessional velocity ( $\leq 2000 \text{ km s}^{-1}$ ) than the majority. Therefore, we may be viewing the projection of two separate systems, or a physical overlap/merger, giving the appearance of a single  $R = 0$  cluster. By subdividing out the galaxies in the following way, a more logical result is obtained:

C1:  $N=3$ ,  $\overline{cz} = 26,285 \text{ km s}^{-1}$ ,  $\sigma = 620 \text{ km s}^{-1}$ ;  
 C2:  $N=5$ ,  $\overline{cz} = 28,275 \text{ km s}^{-1}$ ,  $\sigma = 725 \text{ km s}^{-1}$ .

We note that the dispersions for the two components are still excessive for a Richness 0 cluster. On the other hand, the presence of X-ray emission at the observed level is consistent with a  $R = 1$  or 2 cluster (Ledlow et al. 2003, Figure 9), which lends support to the high velocity dispersions found for the two components. Furthermore, such a large

value of  $L_x$  is also consistent with a cluster merger along the line of sight. In any case, the redshifts of both components are well outside the kinematic core of the HRS.

### 5.2. Abell 3109 (03<sup>h</sup> 16<sup>m</sup>5 –43° 51′0)

Although we add no new observations in this cluster, a compilation of 14 previously published galaxy redshifts provides more established kinematic properties. The ESO Nearby Abell Cluster Survey (ENACS, Katgert et al. 1998) focused on rich clusters with  $R \geq 1$ . The periphery of Abell 3112 (03<sup>h</sup> 17<sup>m</sup>9 –44° 14′0,  $R = 2$ ,  $cz = 22,500$  in Mazure et al. 1996) overlaps with A3109, providing us with 9 redshifts from the ENACS data. The assumed BCG in A3109, 2MASX J03163934–4351169,  $b_J = 15.60$ , has a published redshift of  $18,594 \text{ km s}^{-1}$  (Muriel et al. 1995), which is inconsistent with the published value for the cluster ( $27,581 \text{ km s}^{-1}$  in SR99, see their note).

By incorporating all galaxy redshifts within the prescribed radius, the biweight estimator selects 11 cluster members with the following kinematic properties:  $\overline{cz} = 18,950 \text{ km s}^{-1}$  and  $\sigma = 850 \text{ km s}^{-1}$ . Reducing the radial extent to  $13'$  and thereby excluding 2 proposed members, we obtain a slightly decreased dispersion:  $\overline{cz} = 18,850 \text{ km s}^{-1}$  and  $\sigma = 700 \text{ km s}^{-1}$ . Even though the dispersion remains greater than the  $\sim 400 \text{ km s}^{-1}$  mean for  $R = 0$  clusters that we obtained earlier, the archived redshift information establishes a reliable cluster location (i.e., mean redshift) and places A3109 within the HRS.

### 5.3. Abell 3120 (03<sup>h</sup> 22<sup>m</sup>0 –51° 19′0)

The  $R=0$ ,  $D=5$  cluster, A3120, for which we have obtained 5 galaxy redshifts, is the nearest cluster to the published spatial center of the HRS (Zucca et al. 1993). Its published redshift of  $20,700 \text{ km s}^{-1}$  (SR99) is also close to the  $\sim 19,900 \text{ km s}^{-1}$  mean redshift of the HRS (Paper I). While A3120 does not meet the specific cluster criteria for the APMCC, it does contain the bright galaxy, 2MASX J03215645–5119357 ( $b_J = 15.91$ ), with a previously published redshift of  $21,040 \text{ km s}^{-1}$  (Lucey et al. 1983). The biweight estimator routine accepts all observed galaxies, and we derive the following cluster properties:  $\overline{cz} = 20,525 \text{ km s}^{-1}$ ,  $\sigma = 1400 \text{ km s}^{-1}$ . While the mean derived

velocity is in accord with the published value, the large dispersion is clearly inconsistent with an  $R=0$  cluster. Furthermore, the five galaxies with redshift information show no discernible spatial or kinematic segregation, as one might expect with a cluster. Hence there is reason to suspect that A3120 is not a cluster but the projection of many inter-cluster galaxies near the center of the HRS.

On the other hand, Romer et al. (2000) find X-ray emission at a level of  $L_x = 2.22 \times 10^{43} \text{ ergs s}^{-1}$ , centered on 2MASX J03215645–5119357, and propose that the X-rays are emitted by a “fossil group” (see their Figure 20). These groups form as a result of multiple mergers within the group or a cluster that lead to a single dominant giant elliptical surrounded by an X-ray halo (Ponman et al. 1994; Jones et al. 2003). However, the X-ray position also coincides with a radio source from the Sydney University Molonglo Sky Survey (SUMSS), SUMSS J032156–511935, with a flux density of  $49.0 \text{ mJy}$  (Mauch et al. 2003). Considering the wide range of X-ray luminosities in active galactic nuclei (AGN), it is conceivable that some (or all) of the X-ray emission is a result of the AGN, rather than the fossil halo. Because the galaxy’s redshift is taken from the literature and no optical spectrum is available, we conclude that the situation in A3120 is not soluble with the current observational data. In Table 2 we give the formal mean redshift (location), uncertainty, and dispersion (scale) as deduced from the biweight estimator analysis. However, since we believe that the most likely value of the actual cluster redshift is that of the (presumed) BCG 2MASX J03215645–5119357 ( $cz = 21,040 \text{ km s}^{-1}$ ), we adopt this value for the mean redshift of A3120 in Table 3 (noted by the “1” in column 7). Fortunately, the difference in redshift between  $20,700 \text{ km s}^{-1}$  in Table 2 and  $21,040 \text{ km s}^{-1}$  in Table 3 is within the biweight uncertainty.

## 6. REDSHIFT DISTRIBUTION OF THE HRS CLUSTERS

### 6.1. Consistency with the Inter-cluster Galaxies

In Paper I, the inter-cluster galaxies within the range  $17,000 - 22,500 \text{ km s}^{-1}$  (i.e., the HRS kinematic core) were found to exhibit a systematic  $\sim 1500 \text{ km s}^{-1}$  increase in redshift with position

along a southeast-northwest axis. To quantify this spatial-redshift correlation, we projected the inter-cluster galaxies in the HRS onto an (assumed) principal axis through the spatial center of the HRS. The projected distance along the principal axis was referred to as the  $S$ -coordinate. We then performed a linear correlation analysis between the redshift and the  $S$ -coordinate. After varying the position angle (PA) of the principal axis over the full range of PA and repeating the correlation analysis at each PA, we found that the inter-cluster galaxies show the highest correlation coefficient ( $R = 0.3$ ) and lowest probability for no correlation ( $P < 10^{-6}$ ) at a PA  $\approx -80^\circ$  (as measured east from north). Further details are provided in Paper I. In Figure 2, we plot the projected  $S$  position versus redshift for all inter-cluster galaxies and clusters with redshift between 17,000 and 22,500  $\text{km s}^{-1}$  at a PA of  $-80^\circ$ . As is discussed in Paper I, the distribution of redshifts in Figure 2 is clearly divided into two main components; one centered at  $\sim 18,000 \text{ km s}^{-1}$  and the other at  $\sim 21,000 \text{ km s}^{-1}$ . Furthermore, there is a correlation between the  $S$ -coordinate and redshift for both of the components in the sense that the redshift increases systematically from the southeast (negative  $S$ -coordinate) to the northwest (positive  $S$ -coordinate). Once the kinematic trend is accounted for and removed, the bi-modal nature of the redshift distribution of the inter-cluster galaxies becomes even more apparent. We have plotted the histogram of residual redshifts (after removal of the overall kinematic trend) for the inter-cluster galaxies in the left panel of Figure 3. Using the KMM statistical test (Ashman et al. 1994), we find that a two-gaussian fit to the redshift histogram is preferred to a single gaussian at a confidence level of  $>99.9\%$ .

Although the published cluster redshifts in Paper I followed the spatial-redshift trend of the inter-cluster galaxies, we found that the histogram of residual redshifts showed no evidence for bimodality. This fact appeared somewhat puzzling given the expectation that inter-cluster galaxies and clusters in the same area of the sky should have similar redshift distributions. However, the new cluster redshift data compiled in Table 3 shows a different signature. Plotted as large open circles in Figure 2, the HRS clusters with reliable redshifts now also appear to divide into two

main components. Furthermore, this impression is supported by the histogram of cluster residual redshifts, plotted in the right hand panel of Figure 3. Again, the KMM statistical test is applied to the histogram, and we find that a two-gaussian fit is favored over a single gaussian at the 99.8% confidence level. Moreover, the separation of  $\sim 3000 \text{ km s}^{-1}$  between the two peaks of the cluster redshift distribution is consistent with the similar figure found between the two peaks in the inter-cluster galaxy redshifts. Upon implementing the spatial-redshift correlation analysis described above (i.e., projection of the cluster positional data onto a principal axis), we find a correlation coefficient of  $R = 0.5$  and a probability of no correlation of  $10^{-2}$  at a PA of  $-80^\circ$  for the principal axis. In summary, with the improved mean redshift data for many of the clusters in the HRS, we conclude that the overall redshift distributions of the clusters and the inter-cluster galaxies are now consistent with each other. A closer examination of the inter-relationship between clusters and inter-cluster galaxies in the HRS (e.g., an evaluation as to whether the clusters are indeed located at the intersection of galaxy filaments) awaits a more comprehensive dataset that is in progress.

## 6.2. Re-determination of the Kinematic Core

As mentioned in §2 and above, we determined rough kinematic boundaries in Paper I for the the HRS complex, referred to as the kinematic core, by fitting a gaussian to the redshift distribution of the Abell clusters listed as HRS members by both Zucca et al. (1993) and Einasto et al. (1994). We used the mean redshift and the FWHM of the distribution to define the kinematic core. Given that we now have reliable mean redshifts for 16 of these 17 Abell clusters (we exclude A3120 for reasons discussed in §5.3), it is worth investigating whether the kinematic core changes significantly as a result of the improved redshift data. Using column (6) in Table 3 for the 15 Abell clusters (“A” designation) plus the redshift for A3093 ( $\bar{z} = 24,900 \text{ km s}^{-1}$ , Katgert et al. 1998), the following values for the mean (location) and the dispersion (scale) are obtained by utilizing the bi-weight estimator:  $\bar{z} = 20,150 \pm 525 \text{ km s}^{-1}$  and  $\sigma = 2125 \text{ km s}^{-1}$ . These values imply that the kinematic core of the HRS lies between 17,700 and

22,700 km s<sup>-1</sup>. Hence the kinematic center of the HRS is slightly higher than the previous value, and the core is slightly narrower.

In light of the above discussion, none of our previous results are significantly altered if we use these revised values to define which clusters should be included in the redshift bi-modality analysis. Furthermore, the inter-cluster galaxies from Paper I continue to show a preferred spatial-redshift axis at PA = -80° with similar correlation values over the somewhat-modified range of 17,700 - 22,700 km s<sup>-1</sup>. Moreover, our definition of the kinematic core is only suggestive of what should be included in a detailed analysis of the complex structure of the HRS. Clearly, the actual boundaries of the HRS can be expected to extend to some clusters and inter-cluster galaxies outside the immediate kinematic core.

### 6.3. Comparisons with the Shapley Super-cluster

Finally, we compare the improved cluster redshift distribution for the HRS with that of the Shapley supercluster (hereafter SSC, Quintana et al. 1995, 2000). While the 23 Abell clusters in the SSC for which reliable redshift information is published definitely show a bi-modal distribution, there is a 3:1 number imbalance between the two cluster redshift peaks in the SSC. That is, there are many more clusters in the higher redshift peak, which contains the most massive cluster in the complex, Abell 3558 ( $\bar{cz} = 14,500$  km s<sup>-1</sup>), than there are in the lower redshift peak at  $\sim 11,000$  km s<sup>-1</sup>. In contrast, the HRS clusters are equally split between the two redshift peaks as determined from Figure 3. The difference in mean redshift for the two peaks is slightly higher for the SSC ( $\sim 3500$  km s<sup>-1</sup>) as opposed to the  $\sim 3000$  km s<sup>-1</sup> difference in the HRS. Furthermore, as discussed in Paper I, the redshift distribution for the inter-cluster galaxies in both the HRS and SSC are bi-modal, with a roughly equal split between the two redshift peaks for both clusters (Drinkwater et al. 2004). In short, while there are striking similarities between the two largest mass concentrations in the local universe, the 3:1 imbalance in the number of clusters in the redshift peaks of the SSC represents an interesting contrast with the more evenly distributed HRS.

## 7. CONCLUSIONS

We have obtained 76 new optical redshifts within 12 galaxy clusters of the Horologium-Reticulum supercluster (HRS). These observations, augmented by 42 previously unpublished redshifts, have led to the determination of more accurate cluster properties. Using the methods for calculating robust mean redshifts (location) and velocity dispersions (scale) described in BFG90, we have calculated mean redshifts and dispersions for 13 clusters, including A3109 for which no new observations are reported. The mean redshifts for several clusters have changed by at least 750 km s<sup>-1</sup> (in 6/13 observed) from their previously reported values. In addition, three clusters are observed to consist of multiple components (A3047, A3109, and A3120). The new cluster redshift data have been compared to previously compiled redshift data for the inter-cluster galaxies in the HRS from Fleenor et al. (2005). Primarily, we now find consistency between the large-scale kinematic features of the clusters and the inter-cluster galaxies. Specifically, there is a principal kinematic axis in the HRS at a PA of -80° east from north, along which a systematic increase in redshift with position is observed for both clusters and inter-cluster galaxies. After this overall spatial-kinematic trend is removed, the distribution in redshift for both clusters and inter-cluster galaxies is distinctly bi-modal, with the two redshift peaks separated by  $\sim 3000$  km s<sup>-1</sup>.

We thank the Australian National University and Mount Stromlo/Siding Spring Observatories for facilitating and supporting these observations. We also thank Clair Murrowood for her assistance with the observations, Ilana Klammer for supplying her unpublished 2dF data of A3104, and Bruce Peterson for the use of Mathams' thesis data. M. C. F. acknowledges the support of a NASA Space Grant Graduate Fellowship at the University of North Carolina-Chapel Hill. R. W. H. acknowledges grant support from the Australian Research Council. M. J. H. acknowledges support through IRGS Grant J0014369 administered by the University of Tasmania. A portion of this work was supported by NSF grants AST-9900720 and AST-0406443 to the University of North Carolina-Chapel Hill. This research has made use of the NASA/IPAC Extragalac-



tic Database (NED) which is operated by the Jet Propulsion Laboratory, California Institute of Technology, under contract with the National Aeronautics and Space Administration.

## REFERENCES

- Abell, G. O., Corwin, H. G., & Olowin, R. P. 1989, *ApJS*, 70, 1
- Alonso, M. V., Valotto, C., Lambas, D. G., & Muriel, H. 1999, *MNRAS*, 308, 618
- Ashman, K. A., Bird, C. M., & Zepf, S. E. 1994, *AJ*, 108, 2348
- Bardelli, S., Zucca, E., Zamorani, G., Moscardini, L., & Scaramella, R. 2000, *MNRAS*, 312, 540
- Bardelli, S., Zucca, E., Zamorani, G., Vettolani, G., & Scaramella, R. 1998, *MNRAS*, 296, 599
- Beers, T. C., Flynn, K., & Gebhardt, K. 1990, *AJ*, 100, 32
- Bond, J. R., Kofman, L., & Pogosyan, D. 1996, *Nature*, 380, 603
- Box, G. E. P. 1953, *Biometrika*, 40, 318
- Caldwell, N. & Rose, J. A. 1997, *AJ*, 113, 492
- Colberg, J. M., Krughoff, K. S., & Connolly, A. J. 2005, *MNRAS*, 359, 272
- Colberg, J. M., White, S. D. M., Jenkins, A., & Pearce, F. R. 1999, *MNRAS*, 308, 593
- Colless, M., Dalton, G., Maddox, S., Sutherland, W., Norberg, P., Cole, S., Bland-Hawthorn, J., Bridges, T., Cannon, R., Collins, C., Couch, W., Cross, N., Deeley, K., De Propriis, R., Driver, S. P., Efstathiou, G., Ellis, R. S., Frenk, C. S., Glazebrook, K., Jackson, C., Lahav, O., Lewis, I., Lumsden, S., Madgwick, D., Peacock, J. A., Peterson, B. A., Price, I., Seaborne, M., & Taylor, K. 2001, *MNRAS*, 328, 1039
- Cruddace, R., Voges, W., Böhringer, H., Collins, C. A., Romer, A. K., MacGillivray, H., Yentis, D., Schuecker, P., Ebeling, H., & De Grandi, S. 2002, *ApJS*, 140, 239
- Dalton, G. B., Efstathiou, G., Maddox, S. J., & Sutherland, W. J. 1994, *MNRAS*, 269, 151
- Dalton, G. B., Maddox, S. J., Sutherland, W. J., & Efstathiou, G. 1997, *MNRAS*, 289, 263
- Drinkwater, M. J., Parker, Q. A., Proust, D., Slezak, E., & Quintana, H. 2004, *Publications of the Astronomical Society of Australia*, 21, 89
- Drinkwater, M. J., Proust, D., Parker, Q. A., Quintana, H., & Slezak, E. 1999, *Publications of the Astronomical Society of Australia*, 16, 113
- Einasto, M., Einasto, J., Tago, E., Andernach, H., Dalton, G. B., & Müller, V. 2002, *AJ*, 123, 51
- Einasto, M., Einasto, J., Tago, E., Dalton, G. B., & Andernach, H. 1994, *MNRAS*, 269, 301
- Einasto, M., Einasto, J., Tago, E., Müller, V., & Andernach, H. 2001, *AJ*, 122, 2222
- Einasto, M., Jaaniste, J., Einasto, J., Heinämäki, P., Müller, V., & Tucker, D. L. 2003, *A&A*, 405, 821
- Einasto, M., Tago, E., Jaaniste, J., Einasto, J., & Andernach, H. 1997, *A&AS*, 123, 119
- Fleenor, M. C., Rose, J. A., Christiansen, W. A., Hunstead, R. W., Johnston-Hollitt, M., Drinkwater, M. J., & Saunders, W. 2005, *AJ*, 130, 545
- Gray, P. M. 1983, *Proc. Soc. Photo-opt. Instr. Eng.*, 374, 160
- Grazian, A., Omizzolo, A., Corbally, C., Cristiani, S., Haehnelt, M. G., & Vanzella, E. 2002, *AJ*, 124, 2955
- Hambly, N. C., MacGillivray, H. T., Read, M. A., Tritton, S. B., Thomson, E. B., Kelly, B. D., Morgan, D. H., Smith, R. E., Driver, S. P., Williamson, J., Parker, Q. A., Hawkins, M. R. S., Williams, P. M., & Lawrence, A. 2001, *MNRAS*, 326, 1279
- Hickson, P. 1997, *ARA&A*, 35, 357
- Hudson, M. J., Smith, R. J., Lucey, J. R., Schlegel, D. J., & Davies, R. L. 1999, *ApJ*, 512, L79
- Jones, D. H., Saunders, W., Colless, M., Read, M. A., Parker, Q. A., Watson, F. G., Campbell, L. A., Burkey, D., Mauch, T., Moore, L.,

- Hartley, M., Cass, P., James, D., Russell, K., Fiegert, K., Dawe, J., Huchra, J., Jarrett, T., Lahav, O., Lucey, J., Mamon, G. A., Proust, D., Sadler, E. M., & Wakamatsu, K. 2004, *MNRAS*, 355, 747
- Jones, L. R., Ponman, T. J., Horton, A., Babul, A., Ebeling, H., & Burke, D. J. 2003, *MNRAS*, 343, 627
- Katgert, P., Mazure, A., den Hartog, R., Adami, C., Biviano, A., & Perea, J. 1998, *A&AS*, 129, 399
- Ledlow, M. J., Voges, W., Owen, F. N., & Burns, J. O. 2003, *AJ*, 126, 2740
- Lewis, I. J., Cannon, R. D., Taylor, K., Glazebrook, K., Bailey, J. A., Baldry, I. K., Barton, J. R., Bridges, T. J., Dalton, G. B., Farrell, T. J., Gray, P. M., Lankshear, A., McCowage, C., Parry, I. R., Sharples, R. M., Shortridge, K., Smith, G. A., Stevenson, J., Straede, J. O., Waller, L. G., Whittard, J. D., Wilcox, J. K., & Willis, K. C. 2002, *MNRAS*, 333, 279
- Lucey, J. R., Dickens, R. J., Mitchell, R. J., & Dawe, J. A. 1983, *MNRAS*, 203, 545
- Mauch, T., Murphy, T., Buttery, H. J., Curran, J., Hunstead, R. W., Piestrzynski, B., Robertson, J. G., & Sadler, E. M. 2003, *MNRAS*, 342, 1117
- Mazure, A., Katgert, P., den Hartog, R., Biviano, A., Dubath, P., Escalera, E., Focardi, P., Gerbal, D., Giuricin, G., Jones, B., Le Fevre, O., Moles, M., Perea, J., & Rhee, G. 1996, *A&A*, 310, 31
- Muriel, H., Nicotra, M. A., & Lambas, D. G. 1995, *AJ*, 110, 1032
- Parker, Q. A., Watson, F. G., & Miziarski, S. 1998, in *ASP Conf. Ser. 152: Fiber Optics in Astronomy III*, 80–+
- Pearson, E. S. 1931, *Biometrika*, 21, 114
- Ponman, T. J., Allan, D. J., Jones, L. R., Merrifield, M., McHardy, I. M., Lehto, H. J., & Luppino, G. A. 1994, *Nature*, 369, 462
- Quintana, H., Carrasco, E. R., & Reisenegger, A. 2000, *AJ*, 120, 511
- Quintana, H., Ramirez, A., Melnick, J., Raychaudhury, S., & Slezak, E. 1995, *AJ*, 110, 463
- Romer, A. K., Nichol, R. C., Holden, B. P., Ulmer, M. P., Pildis, R. A., Merrelli, A. J., Adami, C., Burke, D. J., Collins, C. A., Metevier, A. J., Kron, R. G., & Commons, K. 2000, *ApJS*, 126, 209
- Rose, J. A., Gaba, A. E., Christiansen, W. A., Davis, D. S., Caldwell, N., Hunstead, R. W., & Johnston-Hollitt, M. 2002, *AJ*, 123, 1216
- Shapley, H. 1935, *Annals of Harvard College Observatory*, 88, 105
- Struble, M. F. & Rood, H. J. 1999, *ApJS*, 125, 35
- Tonry, J. & Davis, M. 1979, *AJ*, 84, 1511
- Tucker, D. L., Oemler, A. J., Hashimoto, Y., Shectman, S. A., Kirshner, R. P., Lin, H., Landy, S. D., Schechter, P. L., & Allam, S. S. 2000, *ApJS*, 130, 237
- Valdes, F., Gupta, R., Rose, J. A., Singh, H. P., & Bell, D. J. 2004, *ApJS*, 152, 251
- van Haarlem, M. & van de Weygaert, R. 1993, *ApJ*, 418, 544
- West, M. J. & Blakeslee, J. P. 2000, *ApJ*, 543, L27
- Zucca, E., Zamorani, G., Scaramella, R., & Vettolani, G. 1993, *ApJ*, 407, 470

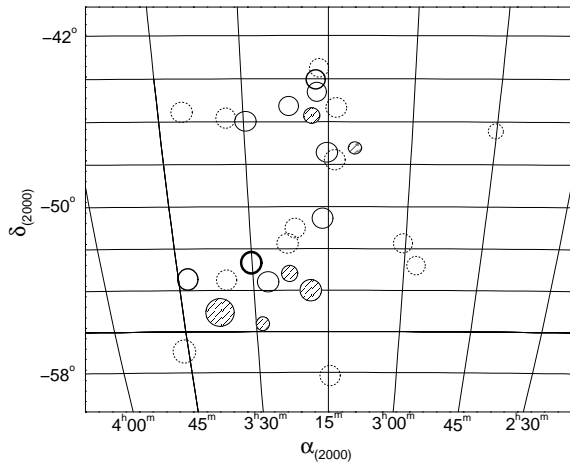


Fig. 1.— Hammer-Aitoff equal-area projection map of the HRS region, with galaxy clusters represented as circles. The radius of each cluster is scaled with the mean redshift to 0.5 Abell radii ( $\sim 1$  Mpc). The thickness of each outline represents the Abell Richness, where thicker lines are clusters of greater Richness Class. Dotted lines are for clusters with previously unreliable redshifts that have been improved in this study. Solid circles represent clusters whose mean redshifts from previous studies are reliable; these clusters are hatched if their redshifts fall outside the kinematic core of the HRS.

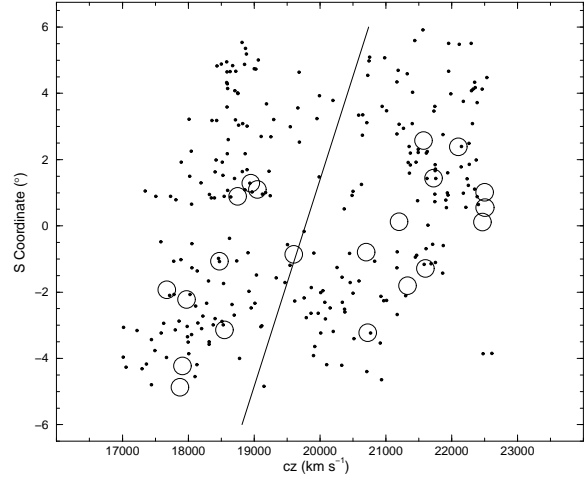


Fig. 2.— Projected angular  $S$ -coordinate is plotted versus redshift for 6dF inter-cluster galaxies from Paper I (small filled circles) between 17,000 and 22,500  $\text{km s}^{-1}$  at a  $\text{PA} = -80^\circ$ . Open circles represent the location and approximate extent of the clusters in the region with mean redshifts listed in Table 3. The solid line is the best fit to the inter-cluster data at this  $\text{PA}$ .

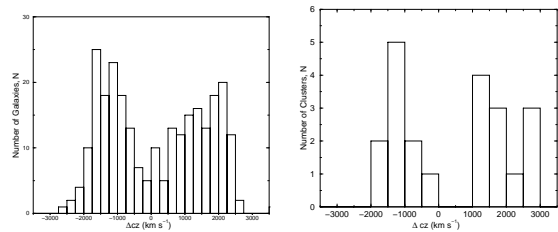


Fig. 3.— Histograms of residual redshifts along the best-fit line at a  $\text{PA} = -80^\circ$ , shown as the solid line in Figure 2. **Left:** Previous results for the HRS inter-cluster galaxies; **Right:** New results for the HRS clusters as listed in Table 3.

TABLE 1  
 REDSHIFT DATA FOR GALAXY CLUSTERS IN HOROLOGIUM-RETICULUM

IAU Name (1)	$\alpha_{2000}$ (2)	$\delta_{2000}$ (3)	$b_J$ (4)	$cz \pm u_{cz}$ (km s $^{-1}$ ) (5)	$cz_{\text{pub}}$ (km s $^{-1}$ ) (6)	Source (7)
Abell 3047						
2MASX J02445221-4630015	02 44 52.22	-46 30 01.3	17.15	26252 $\pm$ 63	26355	1
2MASX J02450315-4628464	02 45 03.10	-46 28 46.2	18.24	28108 $\pm$ 72		
2MASX J02450401-4626435	02 45 03.98	-46 26 43.6	17.56	26921 $\pm$ 72		
2MASX J02450895-4626245	02 45 08.96	-46 26 24.9	18.24	27396 $\pm$ 53		
2MASX J02451207-4628013	02 45 12.14	-46 28 00.9	17.97	28181 $\pm$ 82		
.....	.....	.....	.....	.....	.....	..

NOTE.—Numbers in parentheses apply to column numbers. (1) IAU Name; (2) Right Ascension (J2000); (3) Declination (J2000); (4) SuperCOSMOS  $b_J$  apparent magnitude; (5) radial velocity,  $cz$ , with associated uncertainty; (6) Previously published redshift; (7) Source of published redshift: 1— 6dF observations, unpublished (2004),... Table 1 is published in its entirety in the electronic edition of the *Astronomical Journal*. A portion is shown here for guidance regarding its form and content.

TABLE 2  
 REVISED MEAN REDSHIFTS AND VELOCITY DISPERSIONS FOR HRS CLUSTERS

Cluster (1)	$\alpha_{2000}$ (2)	$\delta_{2000}$ (3)	$N_{\text{gx,prev}}$ (4)	$cz_{\text{prev}}$ (km s $^{-1}$ ) (5)	Source (6)	$N_{\text{gx,new}}$ (7)	$\overline{cz}_{\text{obs}} \pm u_{cz}$ (km s $^{-1}$ ) (8)	$\sigma$ (km s $^{-1}$ ) (9)
A3047	02 45.2	-46 27.0	< 4	28500	1	8	27550: $\pm$ 425	1225:
A3074	02 57.9	-52 43.0	< 4	21900	1	7	21575 $\pm$ 125	325
A3078	03 00.5	-51 50.0	> 0	19440	1	8	22100 $\pm$ 200	575
A3100	03 13.8	-47 47.0	> 0	18870	1	9	19050 $\pm$ 75	250
A3104	03 14.3	-45 24.0	< 4	21885	1	28	21725 $\pm$ 125	700
A3106	03 14.5	-58 05.0	> 0	19170	1	7	19600 $\pm$ 115	300
A3109	03 16.6	-43 51.0	1	27240	2	11	18950: $\pm$ 250	850:
A3120	03 21.9	-51 19.0	> 0	20700	1	5	20525: $\pm$ 675	1400:
A3123	03 23.0	-52 01.0	> 0	19320	1	11	18475 $\pm$ 100	375
A3133	03 32.7	-45 56.0	> 0	16290	1	7	21325 $\pm$ 175	475
APMCC 421	03 35.5	-53 40.9	2	18887	2	11	18550 $\pm$ 100	300
APMCC 433	03 41.1	-45 41.5	2	19786	2	11	20725 $\pm$ 125	425
A3164	03 45.8	-57 02.0	3	17100	1	7	17875 $\pm$ 225	575

NOTE.—Numbers in parentheses apply to column numbers. (1) Cluster name; (2) Right Ascension in hours and minutes (J2000); (3) Declination in degrees and minutes (J2000); (4) Number of galaxies used to establish previously published mean redshift, where “ $N_{\text{gx}} > 0$ ” and “ $N_{\text{gx}} < 4$ ” are designations given by SR99 to reflect the ambiguity regarding the number of individual velocities from the original source; (5) previously published mean redshift; (6) Source for published mean redshift: 1 – SR99 and 2 – Dalton et al. (1994, 1997); (7) Number of galaxies on which the new cluster properties were based; (8) new mean cluster redshift and associated uncertainty; (9) new cluster velocity dispersion.

TABLE 3  
RELIABLE CLUSTER REDSHIFTS IN THE HRS KINEMATIC CORE

Cluster (1)	$\alpha_{2000}$ (2)	$\delta_{2000}$ (3)	Richness (4)	Redshift, $\bar{z}$ (5)	$\overline{cz}$ (km s <sup>-1</sup> ) (6)	$N_{\text{gx}}$ (7)	Source (8)
A3074	02 57.9	-52 43.0	0	0.071917	21575	7	1
A3078	03 00.5	-51 50.0	0	0.073767	22100	8	1
A3100	03 13.8	-47 47.0	0	0.063500	19050	9	1
A3104	03 14.3	-45 24.0	0	0.072417	21725	28	1
A3106	03 14.5	-58 05.0	0	0.065333	19600	7	1
A3108	03 15.2	-47 37.0	1	0.062500	18750	7	2
A3109	03 16.7	-43 51.0	0	0.063167	18950	11	1
A3110	03 16.5	-50 54.0	0	0.074900	22470	10	3
APMCC 369	03 17.5	-44 38.5	0	0.075000	22500	29	3
A3112	03 17.9	-44 14.0	2	0.075000	22500	77	2
S0345	03 21.8	-45 32.3	0	0.070667	21200	18	4
A3120	03 21.9	-51 19.0	0	0.070133	21040	1	5
A3123	03 23.0	-52 01.0	0	0.061583	18475	11	1
A3125	03 27.4	-53 30.0	0	0.058900	17670	40	6
S0356	03 29.6	-45 58.8	0	0.072000	21600	8	3
A3128	03 30.2	-52 33.0	3	0.059900	17970	158	2
A3133	03 32.7	-45 56.0	0	0.071083	21325	7	1
APMCC 421	03 35.5	-53 40.9	0	0.061833	18550	11	1
APMCC 433	03 41.1	-45 41.5	0-1	0.069083	20725	11	1
A3158	03 43.0	-53 38.0	2	0.059700	17910	105	2
A3164	03 45.8	-57 02.0	0	0.059583	17875	7	1

NOTE.—Numbers in parentheses apply to column numbers. (1) Cluster name, where “S” denotes poor clusters from ACO; (2) Right Ascension in hours and minutes (J2000); (3) Declination in degrees and minutes (J2000); (4) ACO Richness or APMCC equivalent; (5) Average redshift taken from Source; (6) Recessional velocity; (7) Number of galaxies used to calculate kinematic properties, for A3120 see §5.3; (8) 1— This study, 2— Katgert et al. (ENACS, 1998), 3— Alonso et al. (1999), 4— I. Klammer (private communication), 5— Lucey et al. (1983), 6—Caldwell & Rose (1997).